

# SIW Cavity Mode Analysis and Control Techniques for Compact Wide-Stopband Filters Design

Daotong Li<sup>1</sup>, Senior Member, IEEE, Wei Luo, Xiaoquan Chen, Jiaxin Wang<sup>2</sup>, Chen Yang, Kai-Da Xu<sup>3</sup>, Senior Member, IEEE, and Qiang Chen<sup>4</sup>, Senior Member, IEEE

**Abstract**—In this brief, a compact novel type of wide-stopband bandpass filter (BPF) is presented based on perturbed dual-mode substrate integrated waveguide (SIW) cavity. The perturbed metallic vias are introduced at the center of SIW cavity to achieve a dual-mode SIW cavity by shifting the resonant frequency of TE<sub>101</sub> mode toward TE<sub>201</sub> mode. Moreover, by setting the external ports to the positions at electric field nulls of the high order spurious modes, the wide-stopband BPF can be realized. Through suppressing the unwanted modes, which includes at least seven modes, the widest stopband up to  $2f_0$  can be obtained in a single SIW cavity. To verify the proposed wide-stopband filter, two prototypes are designed, fabricated and measured, following the stopbands of  $2f_0$  with the rejection level better than 20dB and 30dB, respectively.

**Index Terms**—Bandpass filters (BPFs), dual-mode cavity, perturbed substrate integrated waveguide (SIW), wide-stopband.

## I. INTRODUCTION

WIDE-STOPBAND substrate integrated waveguide (SIW) filters are widely researched and utilized in the modern communication systems, and its characteristics are always constructive with an efficient reduction of the signal interference. SIW technology has also rapidly developed in wireless system due to its high-performance, high-integrity, high power-capacity and low cost. While the spurious passband of SIW filter is close to the fundamental passband, which suffering from a narrow stopband. Therefore, numerous realization methods have been proposed to extend

the stopband [1], [2], [3], [4], [5], [6], [7], [8], [9], [10], [11], [12], [13], [14], [15], [16], [17].

The conventional approach to improve the stopband is cascading low-pass filter [1], which results in a large circuit size and a deteriorated insertion loss. To realize more compact size, the cross coupling and mixed coupling are widely used methods to introduce transmission zeros (TZs) out of band [2], [3], [4], [5]. Nonetheless, the stopband is also limited due to the narrowly spaced TZs. Moreover, through controlling the shape of the SIW cavities and the region of inner coupling [6], [7], [8], [9], [10], the wide-stopband and high suppression can also be achieved. However, there is a common problem in the above-mentioned literatures that they all use only one resonant mode and the higher resonant modes are supposed to be suppressed to improve the stopband. As seen in [6], a fourth-order wide-stopband filter is realized by centered I/O ports and coupling windows. The stopband can be extended to  $2.5f_0$  under 25 dB, but the circuit size is up to  $2.87\lambda_g^2$ .

As well as we known, it is rarely reported the dual-mode SIW wide-stopband BPFs. In [11], a dual-mode filter is designed with multiple TZs to improve the performance of stopband. The suppression level is up to 48 dB while the bandwidth of stopband is limited to  $1.28f_0$ . In [12], [13] the suppression method by cascading single mode SIW cavities with a dual-mode SIW cavity has been employed to extend the stopband, while the stopband can merely extend to  $1.28f_0$  below 20 dB and  $1.67f_0$  below 20 dB, respectively, and large circuit sizes are unavoidable. According to the research, the stopband is hardly to reach  $2f_0$  when the filter is based on a dual-mode SIW cavity. As for other wide-stopband BPFs using single mode SIW cavity. In [14], [15], the wide-stopband filters are designed using just fundamental mode, and through cascading SIW cavities to extend the stopband to  $1.95f_0$  below 50dB and  $2.5f_0$  below 25dB, respectively. While the narrow bandwidth and large circuit size are obtained. In [16], [17], compact wide-stopband filters can be achieved, while the hybrid structure by combing SIW cavity and microstrip technology is very complex.

In this brief, a novel dual-mode SIW BPF using a single perturbed SIW cavity is proposed. Moreover, the filter can realize a wide-stopband compared with other reported dual-mode works. The basic structure is a dual-mode SIW cavity based on both TE<sub>101</sub> and TE<sub>201</sub> modes, and the unwanted modes in the cavity are expected to be suppressed by arranging the external ports at the regions of electric field nulls of these modes, and at least seven modes are rejected in a single cavity. Second- and fourth-order SIW BPFs are

Manuscript received 16 December 2023; revised 24 January 2024; accepted 2 February 2024. Date of publication 12 February 2024; date of current version 1 July 2024. This work was supported in part by the FY2021 JSPS Postdoctoral Fellowship for Research in Japan under Grant P21053; in part by the Grant-in-Aid for JSPS Research Fellow under Grant 21F21053; in part by the National Natural Science Foundation of China under Grant 61801059; and in part by the Basic Research and Frontier Exploration Special of Chongqing Natural Science Foundation under Grant cstc2019jcyj-msxmX0350. This brief was recommended by Associate Editor Q. Feng. (Corresponding author: Daotong Li.)

Daotong Li is with the School of Microelectronics and Communication Engineering, Chongqing University, Chongqing 400044, China, and also with the Research Institute for Sustainable Humansphere, Kyoto University, Kyoto 606-8501, Japan (e-mail: dli@cqu.edu.cn).

Wei Luo, Xiaoquan Chen, Jiaxin Wang, and Chen Yang are with the School of Microelectronics and Communication Engineering, Chongqing University, Chongqing 400044, China.

Kai-Da Xu is with the School of Information and Communications Engineering, Xi'an Jiaotong University, Xi'an 710049, China.

Qiang Chen is with the Department of Communications Engineering, Tohoku University, Sendai 980-8579, Japan.

Color versions of one or more figures in this article are available at <https://doi.org/10.1109/TCSII.2024.3364816>.

Digital Object Identifier 10.1109/TCSII.2024.3364816

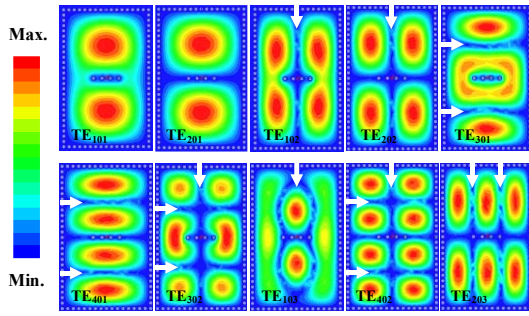


Fig. 1. Electric field distribution of the first several modes in the perturbed SIW cavity. (The arrows indicate the external or internal coupling positions.).

designed for demonstration, and their stopbands extend to  $2f_0$  with the rejection levels better than 20 dB and 30dB, respectively.

## II. PROPOSED DUAL-MODE SIW CAVITY AND THE SUPPRESSION TECHNIQUE

### A. Perturbed SIW Cavity and Suppression Technology

Fig. 1 shows the electric field distributions of the first several resonant modes in the perturbed SIW cavity, where the arrows indicate the external or internal coupling position for the suppression of spurious modes. As is known to all, setting the external feeding port or the internal coupling windows at the weakest position of the electric fields can be applied to reach wide-stopband of SIW BPFs. However, the traditional wide-stopband filters are based on single-mode resonators and through cascading several cavities to extend the stopband. The stopband improvements in a single SIW cavity have not yet been considered. The external coupling ports are expected not only to excite  $TE_{101}$  and  $TE_{201}$  modes, but also should be coupled at the regions where the electric field distributions of higher modes are weakest. Therefore, the external ports are impossible to be placed at opposite sides to satisfy the passband and stopband simultaneously. For instance, if  $TE_{102}$  and  $TE_{202}$  modes have to be rejected, the external port should be placed at the center of the bottom sidewall. Similarly, when  $TE_{401}$  mode needs to be suppressed, the external port should be coupled at one quarter of the left sidewall. Moreover, if the external port is arranged at the one quarter of the left sidewall or one half of the bottom sidewall, the  $TE_{402}$  mode will be rejected. The electric field distributions of  $TE_{301}$  and  $TE_{103}$  modes are perturbed due to the metallic vias structure, which creates an opportunity for suppression. The difference in this dual-mode cavity is that the first two resonant modes, both  $TE_{101}$  and  $TE_{201}$ , are utilized to form the passband.

The prototype is implemented on Rogers RT/Duriod 5880 substrate with the relative dielectric constant  $\epsilon_r = 2.2$ , thickness  $h = 0.508$  mm, and  $\tan \delta = 0.0009$ , while the diameter of the via-holes  $d = 0.6$  mm and center to center pitch  $p = 1$  mm are selected.

To extend the stopband as wide as possible, the unwanted modes should stay away from the fundamental mode. The resonant frequency ratios of the higher order modes to the

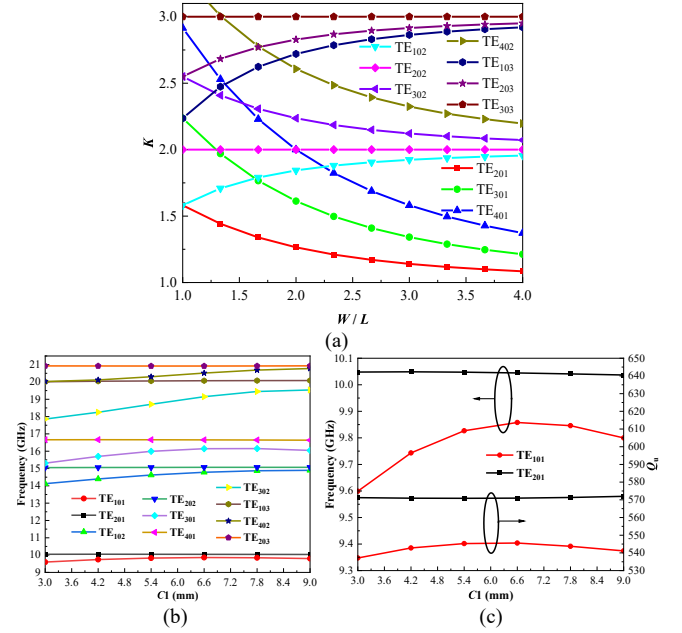


Fig. 2. (a) Normalized resonant frequencies of the first several modes in the rectangular cavity against  $W/L$  without metallic vias perturbation structure, and (b) simulated frequencies of first ten modes and (c) the in-band two modes and unload  $Q$ -factors against  $C1$  in the perturbed SIW cavity.

fundamental mode are decided by

$$k = \frac{f_{TE_{m0n}}}{f_{TE_{101}}} = \sqrt{n^2 + \frac{m^2 - n^2}{1 + \left(\frac{W}{L}\right)^2}}, \quad (1)$$

where  $m$  and  $n$  are the mode indices while  $W$  and  $L$  are the physical width and length of the rectangular cavity. The frequency ratio  $k$  versus  $W/L$  has been depicted in Fig. 2(a). As can be seen,  $k$  will gradually increase with  $W/L$  increasing when  $m < n$ , and decrease when  $m > n$ . While  $m = n$ , the ratio  $k$  is constant. Therefore, a suppression strategy is adjusting  $W/L$  to shift the unsuppressed modes toward higher frequency to improve the stopband, and  $TE_{103}$  is the first mode that cannot be rejected from the formula. Owing to the perturbation, the resonant frequency of  $TE_{101}$  mode shifts toward  $TE_{201}$  mode to form a dual-mode cavity. The  $TE_{201}$  mode can be considered as the fundamental mode as it is not affected by the metallic vias, and the resonant frequency of  $TE_{402}$  mode is twice as much as  $TE_{201}$  mode from the formula.

To comprise the dual-mode SIW cavity, the metallic vias are placed at the center of the cavity. The simulated frequencies of the first ten modes and in-band two modes with unload  $Q$ -factors against the parameter  $C1$  in the perturbed SIW cavity are shown in Fig. 2(b) and (c). As can be seen from Fig. 2(b), the resonant frequencies of  $TE_{201}$ ,  $TE_{202}$ ,  $TE_{401}$ ,  $TE_{402}$  and  $TE_{203}$  modes keep steady, which benefits from the electric field distributions of these modes are not disturbed by metallic vias. On the other hand, the resonant frequencies of  $TE_{101}$ ,  $TE_{102}$ ,  $TE_{301}$ ,  $TE_{302}$  and  $TE_{103}$  modes gradually shift toward higher frequencies as the parameter  $C1$  increases. The resonant frequency of  $TE_{101}$  mode increases firstly and then decreases while  $TE_{201}$  keeps almost constant when  $C1$  changes from 3 to 9 mm, because the metallic vias only perturb

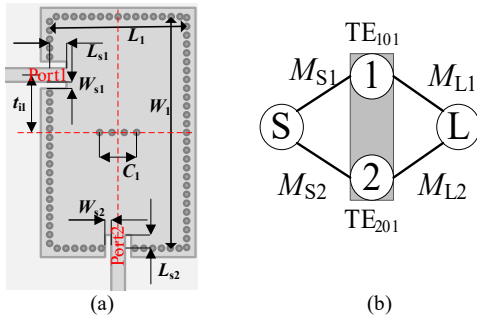


Fig. 3. (a) Geometric configurations and (b) topology of the second-order wide-stopband SIW BPFs.

TE<sub>101</sub> mode while TE<sub>201</sub> mode is not disturbed. Moreover, the bandwidth mainly depends on the frequency spacing between TE<sub>101</sub> and TE<sub>201</sub> modes, which could also be controlled by C1.

### B. Implementation of the Second-Order BPF

To validate the theory, a second-order wide-stopband SIW BPF is designed. The geometry of the second-order wide-stopband filter based on the perturbed SIW cavity is shown in Fig. 3(a). Several metallic vias are placed along the horizontal center line of the rectangular cavity to perturb the TE<sub>101</sub>, TE<sub>301</sub>, TE<sub>302</sub> and TE<sub>103</sub> modes, and the resonant frequency of TE<sub>101</sub> mode shifts toward TE<sub>201</sub> mode to form the passband. There are just two external ports are available to reject spurious modes. The topology of the proposed structure is illustrated in Fig. 3(b), where nodes 1 and 2 represent the TE<sub>101</sub> and TE<sub>201</sub> modes, respectively. Nodes S and L represent the input and output ports, respectively. Due to the electric field distributions of the TE<sub>101</sub> and TE<sub>201</sub> modes in Fig. 1,  $M_{S1}$  and  $M_{L1}$  have the identical signs (i.e.,  $M_{S1} = M_{L1}$ ), whereas  $M_{S2}$  and  $M_{L2}$  have opposite signs (i.e.,  $M_{S2} = -M_{L2}$ ). A TZ outside the passband can be introduced whenever  $M_{S1} \neq M_{S2}$ , and the position of the TZ is determined by the ratio  $M_{S2}/M_{S1}$ . The ratio is controlled by the offset of Port 1 or Port 2, and  $M_{S1}$  is always larger than  $M_{S2}$ , which results in the TZ only occurring in the upper stopband.

For the second-order BPF, if the input Port 1 is placed at one-quarter of left sidewall, the TE<sub>m0n</sub> ( $m = 4, 8, \dots$ ) modes in the SIW cavity will be naturally rejected. On the other hand, Port 2 is arranged at the center of bottom sidewall to reject the TE<sub>m0n</sub> ( $n = 2, 4, \dots$ ) modes. To illustrate the offset influence of two external ports, Fig. 4 has shown the simulated frequency responses versus different parameters of  $t_{11}$  and  $t_{12}$ . As can be seen in Fig. 4(a) and Fig. 1, the TE<sub>301</sub> and TE<sub>401</sub> modes cannot be suppressed when the offset  $t_{11}$  is far away from the predetermined region (one-quarter of left sidewall). However, one TZ can be generated above the passband due to the coupling strengths  $M_{S1}$  and  $M_{S2}$  are not equal, and gradually moving toward a higher frequency until it disappears when  $M_{S1} = M_{S2}$  as  $t_{11}$  increases. Moreover, when the Port 2 is not at the center of the bottom sidewall, the TE<sub>102</sub>, TE<sub>202</sub> and TE<sub>103</sub> modes will be fully excited by Port 1 and transmitted to Port 2 that demonstrates in Fig. 4(b). Actually, the TE<sub>301</sub> and TE<sub>103</sub> modes cannot be rejected in the normal SIW cavity if the metallic vias are not introduced into

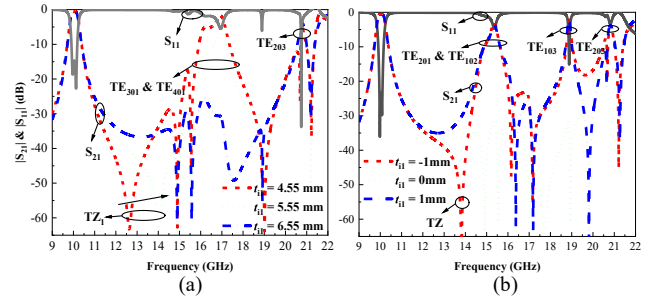


Fig. 4. Simulated frequency responses of two poles SIW wide-stopband filter versus different (a)  $t_{11}$  as a fixed  $t_{12} = 0$  mm and (b)  $t_{12}$  as a fixed  $t_{11} = 6.55$  mm.

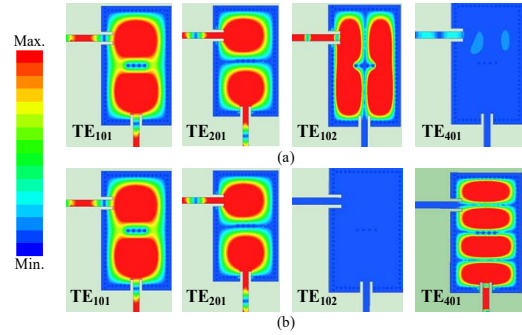


Fig. 5. Electric field distributions in the second-order wide-stopband SIW filter with the excitation of (a) Port 1 and (b) Port 2 at  $f_{TE_{101}}$ ,  $f_{TE_{201}}$ ,  $f_{TE_{102}}$  and  $f_{TE_{401}}$ , respectively.

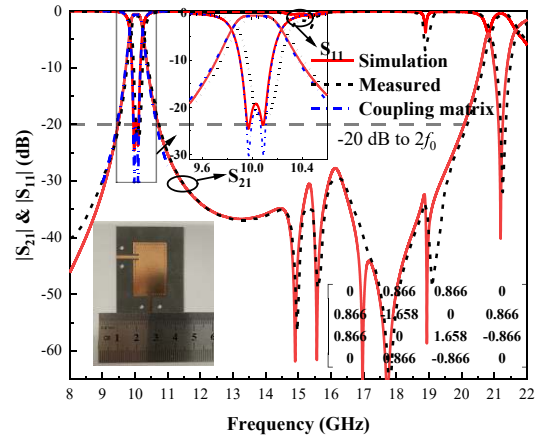


Fig. 6. The simulated and measured frequency responses of two-poles wide-stopband BPF with the inserted photograph of the fabricated object.

the cavity. Through tuning the region of two external ports, the whole resonant modes between TE<sub>201</sub> and TE<sub>203</sub> modes can be well suppressed and the stopband can be extended to 20 GHz.

Fig. 5 demonstrates the electric field distributions in the second-order wide-stopband SIW filter with the excitation of Port 1 and Port 2 at  $f_{TE_{101}}$ ,  $f_{TE_{201}}$ ,  $f_{TE_{102}}$  and  $f_{TE_{401}}$ , respectively. As can be seen, TE<sub>101</sub> and TE<sub>201</sub> modes in the single SIW cavity comprise the passband regardless of the excitation ports. Nonetheless, when setting Port 1 as excitation port, TE<sub>102</sub> mode could be excited but could not be transmitted to Port 2, while TE<sub>401</sub> mode could not be excited as illustrated in

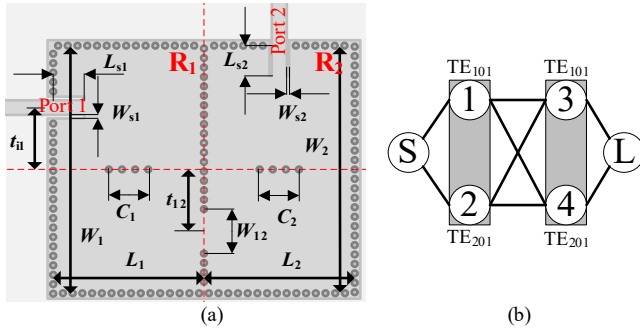


Fig. 7. (a) Geometric configurations and (b) topology of the fourth-order wide-stopband SIW BPFs.

Fig. 6(a). When setting Port 2 as excitation port,  $TE_{102}$  mode could not be excited, while  $TE_{401}$  mode could be excited but could not be transmitted to Port 1 as illustrated in Fig. 6(b). Therefore, both  $TE_{102}$  and  $TE_{401}$  modes could be suppressed, which is also suitable for other resonant modes.

Fig. 6 shows the simulated and measured results with the inserted photograph of the fabricated second-order wide-stopband BPF. The final dimensions are given as follows:  $W_1 = 26.2$  mm,  $L_1 = 15.5$  mm,  $C_1 = 2.1$  mm,  $t_{11} = 6.5$  mm,  $L_{s1} = 1.9$  mm,  $L_{s2} = 1.5$  mm,  $W_{s1} = 0.75$  mm,  $W_{s2} = 0.7$  mm. The filter is centered at 10 GHz with a 3-dB bandwidth and fractional bandwidth (FBW) of 375 MHz and 3.75%, respectively. The measured return loss is better than 20 dB, and the minimum insertion loss is 1.92 dB. The measured stopband can be extended up to 20 GHz with the suppression level below 20 dB, and 19.5 GHz with the suppression level below 25dB. The whole circuit size is about  $0.77 \lambda_g \times 1.29 \lambda_g$ . To the author's knowledge, this design is firstly investigated to reach wide-stopband up to  $2f_0$  in a single dual-mode SIW cavity.

### III. DESIGN AND IMPLEMENTATION OF FOUR-POLE WIDE-STOPBAND BPF

To further improve the passband selectivity, a fourth-order wide-stopband SIW BPF is realized through cascading two similar perturbed dual-mode SIW cavities  $R_1$  and  $R_2$ , the geometric configurations and topology are shown in Fig. 7. As demonstrated in Fig. 7(a), Port 1 is still arranged at one-quarter of left sidewall of  $R_1$ , and Port 2 is placed at the center of top sidewall of  $R_2$ . The inner coupling between two dual-mode SIW cavities  $R_1$  and  $R_2$  is executed by a coupling window, which is deviated from the central line of the two cavities. The coupling strength of the  $TE_{101}$  and  $TE_{201}$  modes in two cavities is determined by the offset  $t_{12}$  and the width  $W_{12}$ . It is worth mentioning that the coupling ratio between source and first two modes is mainly decided by the offset  $t_{12}$ , while the coupling strength is mainly decided by coupling width  $W_{12}$ . The coupling window is arranged along the vertical central line not only as a port of  $R_1$  or  $R_2$ , but also has to suppress the higher-order resonant modes.

It can be observed that there are two extra TZs above the passband compared with the second-order filter. The first TZ is close to the passband, which can enhance the selectivity of the filter, and the second TZ is far away from the passband which can be used to improve the performance of stopband.

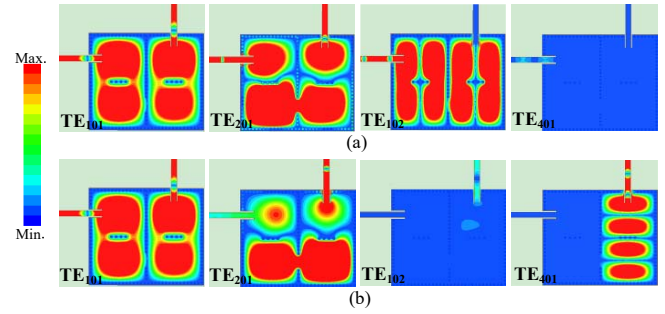


Fig. 8. Electric field distributions in the fourth-order wide-stopband SIW filter with the excitation of (a) Port 1 and (b) Port 2 at  $f_{TE_{101}}$ ,  $f_{TE_{201}}$ ,  $f_{TE_{102}}$  and  $f_{TE_{401}}$ , respectively.

The position of the first TZ is depended on the coupling ratio between source and  $TE_{101}$  and  $TE_{201}$  modes which can be controlled by offset  $t_{11}$ . While the second TZ is introduced and determined by the bypass coupling through higher modes. It is worth mentioning that both TZs are introduced by the first perturbed dual-mode SIW cavity  $R_1$ , while the second cavity  $R_2$  will not generate TZ that similar with the second-order wide-stopband filter in Section II.

Fig. 8 demonstrates the electric field distributions in the fourth-order wide-stopband SIW filter with the excitation of Port 1 and Port 2 at  $f_{TE_{101}}$ ,  $f_{TE_{201}}$ ,  $f_{TE_{102}}$  and  $f_{TE_{401}}$ , respectively. Similarly,  $TE_{101}$  and  $TE_{201}$  modes in each SIW cavity form the passband. When setting Port 1 as excitation port,  $TE_{102}$  mode could be excited in both  $R_1$  and  $R_2$  but could not be transmitted to Port 2, while  $TE_{401}$  mode could not be excited as shown in Fig. 8(a). When setting Port 2 as excitation port,  $TE_{102}$  mode could not be excited, while  $TE_{401}$  mode could be excited in  $R_2$  but could not transmitted to  $R_1$ , which is suppressed by the inner coupling window as shown in Fig. 8(b). Therefore, both  $TE_{102}$  and  $TE_{401}$  modes could be rejected.

Fig. 9(a) shows the variation in the bandwidth of passband against  $t_{12}$  and  $W_{12}$ , respectively. As can be seen, when the parameter  $t_{12}$  increases from 4.55mm to 6.55mm with a fixed  $W_{12}$ , the bandwidth of passband is slightly changed. On the contrary, when the parameter  $W_{12}$  increases from 4.2mm to 5.2mm with a fixed  $t_{12}$ , the bandwidth of passband becomes wider. Fig. 9(b) shows the simulated and measured results with the inserted photograph of the fabricated fourth-order wide-stopband filter. The final dimensions are given as follows:  $W_1 = W_2 = 26.2$  mm,  $L_1 = L_2 = 15.5$  mm,  $C_1 = C_2 = 2.1$  mm,  $t_{11} = 6.55$  mm,  $L_{s1} = L_{s2} = 3.2$  mm,  $W_{s1} = 0.38$  mm,  $W_{s2} = 0.23$  mm,  $t_{12} = 6.55$  mm, and  $W_{12} = 4.71$  mm. The measured filter is centered at 10 GHz with a 3-dB bandwidth and FBW of 400 MHz and 4%, respectively. The measured return loss is better than 20 dB, and the minimum insertion loss is 1.98 dB. As can be seen from the results, there are two more transmission zeros above the passband which are separately located at 11.45 and 13.67 GHz. The measured stopband can be extended up to 20 GHz with the suppression level below 30 dB, and 14 GHz with the suppression level below 50 dB. The whole circuit size is about  $1.54 \lambda_g \times 1.29 \lambda_g$ .

The comparisons with other wide-stopband SIW BPFs are listed in Table I to highlight the performance of the proposed filters. The proposed wide-stopband filters realize a

TABLE I  
COMPARISON WITH OTHER WIDE-STOPBAND SIW FILTERS

Ref.	$f_0$ (GHz)	FBW (%)	NM	NP	NZ	IL (dB)	R.L. (dB)/Stopband	Size ( $\lambda_g^2$ )
[12]	15	4.3	2	4	5	1.7	48 / $1.28f_0$	3.02
[13]	12.47	3.74	2	4	2	1.34	20 / $1.28f_0$	2.77
[14]	10	3.98	2	4	1	1.52	20 / $1.67f_0$	1.98
[16]	6.5	1.92	1	2	0	2.52	25 / $2.5f_0$	1.23
[18]	10.11	11.7	1	4	2	1.22	20 / $2.9f_0$	1.08
Filter I	10	3.75	2	2	0	1.92	20 / $2f_0$	0.99
Filter II	10	4	2	4	2	1.98	30 / $2f_0$	1.98

$f_0$ : center frequency; FBW: fractional bandwidth; NM: number of utilized resonant modes; NP: number of poles; NZ: number of TZs;  $\lambda_g$ : guided wavelength in the dielectric substrate at  $f_0$ .

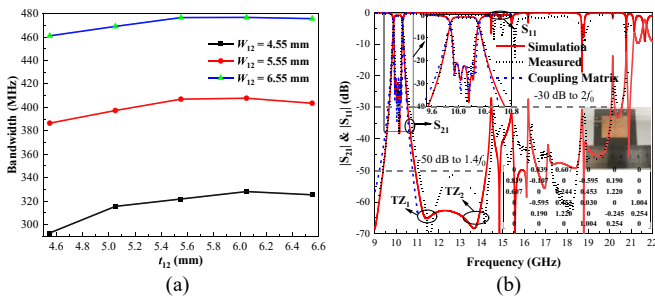


Fig. 9. (a) The variation in the bandwidth of passband against  $t_{12}$  and  $W_{12}$ , respectively, and (b) the simulated and measured frequency responses of four-poles wide-stopband BPF with the inserted photograph of the fabricated object.

more compact circuit size, a wider bandwidth, and a better performance of stopband simultaneously. Moreover, a single dual-mode SIW cavity BPF with wide-stopband is achieved in this brief, and easier to achieve higher-order BPFs.

#### IV. CONCLUSION

This brief demonstrates a novel type of wide-stopband BPFs by using perturbed dual-mode SIW cavity with simple design structure. Both of  $TE_{102}$  and  $TE_{201}$  modes are utilized to comprise the passband, while the wide-stopband is realized using mode analysis and control technique. At least seven resonant modes between  $TE_{201}$  and  $TE_{203}$  modes are suppressed to enhance the stopband performance. Two prototypes, including two- and four-pole BPFs centered at 10 GHz, have been designed, fabricated and measured to illustrate the validity of the proposed dual-mode structure, demonstrating a more compact size and the stopband can be extended to  $2f_0$  below 20 and 30 dB, respectively.

#### REFERENCES

- [1] S. Y. Zheng, Z. L. Su, Y. M. Pan, Z. Qamar, and D. Ho, "New dual-/tri-band bandpass filters and diplexer with large frequency ratio," *IEEE Trans. Microw. Theory Techn.*, vol. 66, no. 6, pp. 2978–2992, Jun. 2018.
- [2] A. R. Azad and A. Mohan, "Substrate integrated waveguide dual-band and wide-stopband bandpass filters," *IEEE Microw. Wireless Compon. Lett.*, vol. 28, no. 8, pp. 660–662, Aug. 2018.
- [3] C.-X. Zhou, P.-P. Guo, K. Zhou, and W. Wu, "Design of a compact UWB filter with high selectivity and superwide stopband," *IEEE Microw. Wireless Compon. Lett.*, vol. 27, no. 7, pp. 636–638, Jul. 2017.
- [4] Z. L. Su, B. W. Xu, S. Y. Zheng, H. W. Liu, and Y. L. Long, "High-isolation and wide-stopband SIW diplexer using mixed electric and magnetic coupling," *IEEE Trans. Circuits Syst. II, Exp. Briefs*, vol. 67, no. 1, pp. 32–36, Jan. 2020.
- [5] K. F. Chen, X. Yang, L. Zhou, and J.-F. Mao, "Miniaturized half-mode T-septum SIW bandpass filter with an ultrawide stopband," *IEEE Microw. Wireless Compon. Lett.*, vol. 31, no. 7, pp. 853–856, Jul. 2021.
- [6] K. Zhou, C.-X. Zhou, and W. Wu, "Resonance characteristics of substrate-integrated rectangular cavity and their applications to dual-band and wide-stopband bandpass filters design," *IEEE Trans. Microw. Theory Techn.*, vol. 65, no. 5, pp. 1511–1524, May 2017.
- [7] H.-W. Xie, K. Zhou, C.-X. Zhou, and W. Wu, "Compact SIW diplexers and dual-band bandpass filter with wide-stopband performances," *IEEE Trans. Circuits Syst. II, Exp. Briefs*, vol. 67, no. 12, pp. 2933–2937, Dec. 2020.
- [8] P. Chu, J. Feng, L. Guo, L. Zhang, L. Liu, and K. Wu, "Multilayer substrate integrated waveguide filter with multimode suppression and wide stopband," *IEEE Trans. Circuits Syst. II, Exp. Briefs*, vol. 69, no. 11, pp. 4553–4557, Nov. 2022.
- [9] A. Iqbal, A. W. Ahmad, A. Smida, and N. K. Mallat, "Tunable SIW bandpass filters with improved upper stopband performance," *IEEE Trans. Circuits Syst. II, Exp. Briefs*, vol. 67, no. 7, pp. 1194–1198, Jul. 2020.
- [10] D. Ma, K. Zhou, H. Xie, T. Huang, and W. Wu, "Compact or wide-stopband SIW diplexers with high intrinsic isolations based on orthogonal dual modes," *IEEE Trans. Circuits Syst. II, Exp. Briefs*, vol. 70, no. 1, pp. 71–75, Jan. 2023.
- [11] P. Chu et al., "Dual-mode substrate integrated waveguide filter with flexible response," *IEEE Trans. Microw. Theory Techn.*, vol. 65, no. 3, pp. 824–830, Mar. 2017.
- [12] Q. Liu, D. Zhou, Y. Zhang, D. Zhang, and D. Lv, "Substrate integrated waveguide bandpass filters in box-like topology with bypass and direct couplings in diagonal cross-coupling path," *IEEE Trans. Microw. Theory Techn.*, vol. 67, no. 3, pp. 1014–1022, Mar. 2019.
- [13] Q. Liu, D. Zhang, M. Tang, H. Deng, and D. Zhou, "A class of box-like bandpass filters with wide stopband based on new dual-mode rectangular SIW cavities," *IEEE Trans. Microw. Theory Techn.*, vol. 69, no. 1, pp. 101–110, Jan. 2021.
- [14] P. Chu, L. Guo, L. Zhang, F. Xu, W. Hong, and K. Wu, "Wide stopband substrate integrated waveguide filter implemented by orthogonal ports' offset," *IEEE Trans. Microw. Theory Techn.*, vol. 68, no. 3, pp. 964–970, Mar. 2020.
- [15] H.-W. Xie, K. Zhou, C.-X. Zhou, and W. Wu, "Wide-stopband SIW filters using modified multi-spurious modes suppression technique," *IEEE Trans. Circuits Syst. II, Exp. Briefs*, vol. 67, no. 12, pp. 2883–2887, Dec. 2020.
- [16] G. Lin, Y. Dong, and X. Luo, "Miniaturized quarter-mode SIW filters loaded by dual-mode microstrip resonator with high selectivity and flexible response," *IEEE Microw. Wireless Compon. Lett.*, vol. 32, no. 6, pp. 660–663, Jun. 2022.
- [17] Y. Zhu and Y. Dong, "A novel compact wide-stopband filter with hybrid structure by combining SIW and microstrip technologies," *IEEE Microw. Wireless Compon. Lett.*, vol. 31, no. 7, pp. 841–844, Jul. 2021.